NANO LETTERS

February 22, 2023
Volume 23, Number 4
pubs.acs.org/NanoLett

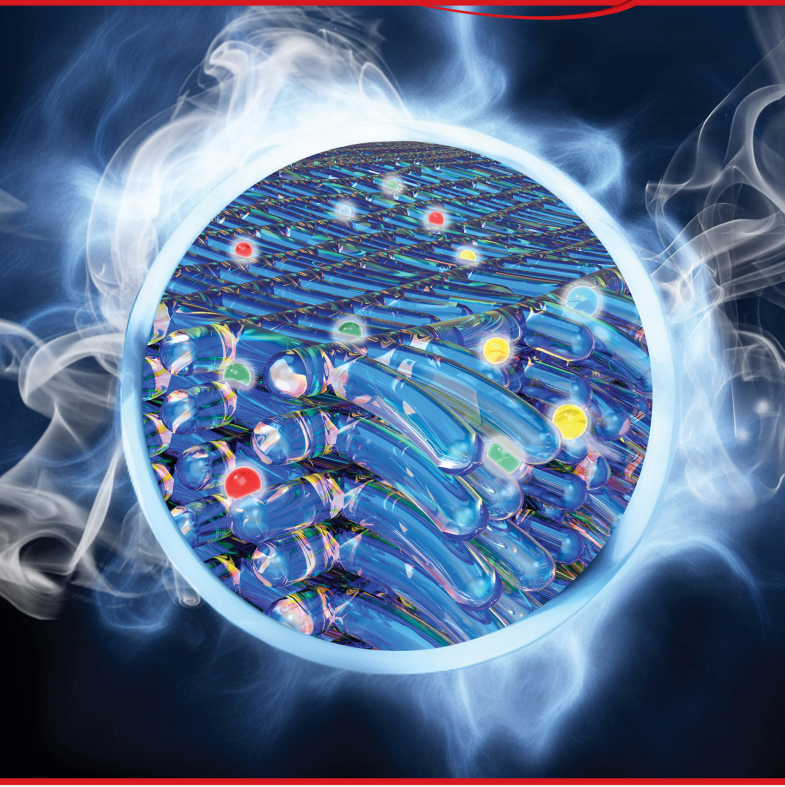

ACS Publications
Most Trusted. Most Cited. Most Read.

www.acs.org

NANO LETTERS

pubs.acs.org/NanoLett

Letter

Pencil-on-Paper Humidity Sensor Treated with NaCl Solution for Health Monitoring and Skin Characterization

Guangyu Niu,[¶] Zihan Wang,[¶] Ye Xue, Jiayi Yan, Ankan Dutta, Xue Chen, Ya Wang, Chaosai Liu, Shuaijie Du, Langang Guo, Peng Zhou, Huanyu Cheng,* and Li Yang*

Cite This: *Nano Lett.* 2023, 23, 1252−1260

Read Online

ACCESS | Metrics & More | Article Recommendations | Supporting Information

ABSTRACT: Although flexible humidity sensors are essential for human health monitoring, it is still challenging to achieve high sensitivity and easy disposal with simple, low-cost fabrication processes. This study presents the design and fabrication of highly reliable hand-drawn interdigital electrodes from pencil-on-paper treated with NaCl solution for highly sensitive hydration sensors working over a wide range of relative humidity (RH) levels from 5.6% to 90%. The applications of the resulting flexible humidity sensor go beyond the monitoring of respiratory rate and proximity to characterizations of human skin types and evaluations of skin barrier functions through insensible sweat measurements. The sensor array can also be integrated with a diaper to result in smart diapers to alert for an early diaper change. The design and fabrication strategies presented in this work could also be leveraged for the development of wearable, self-powered, and recyclable sensors and actuators in the future.

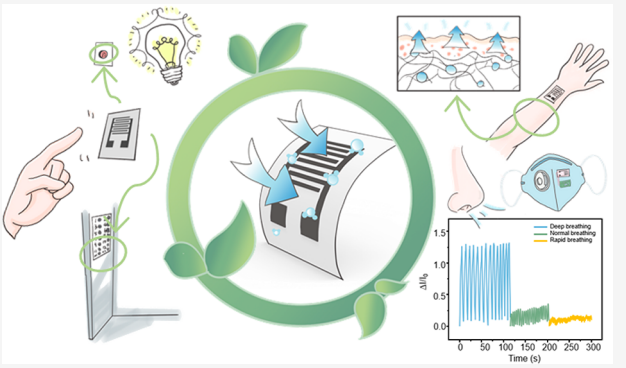

KEYWORDS: *flexible humidity sensors and sensing systems, pencil-on-paper, characterizations of skin types and barrier functions, monitoring of sensible and insensible sweat rate*

The recent developments of wearable sensors have started to gain momentum because of their wide-ranging applications in medical health,[1] disaster warning,[2] and military defense.[3] As representative examples, flexible humidity sensors have been applied in environment monitoring,[4] product packaging,[5] and human health care,[6] such as respiratory monitoring,[7] noncontact positioning,[8] and skin humidity detection.[9] The commonly explored substrates for flexible sensors include polyimide, polyester, and polyethylene terephthalate,[10−12] as well as cellulose types, including cellulose fibers,[13,14] fabrics,[15] and various papers.[16−19] In particular, low-cost and environmentally friendly papers[20] that are compatible with most preparation processes[21] can also be used as sensitive materials for humidity sensors by leveraging their hygroscopic properties for reversible moisture absorption (to measure respiratory patterns[22]).

Besides the flexible substrate and sensitive material, the electrode and corresponding fabrication process also affect the performance and scalability. Traditional electrode fabrication processes such as inkjet printing,[23,24] screen printing,[25] and electrochemical deposition[26] often require expensive equipment and are not environmentally friendly. However, scratching pencils (composed of graphite and clay) by hand drawing can cause a small number of multilayered graphite pieces to flake and form electrodes on paper with a mask.[27] As the conductance of the pencil core increases and then saturates with the increasing graphite content, the electrode prepared with an 8B pencil shows the smallest square resistance.[28] Nevertheless, the resulting draw-on-paper electrodes still need to be combined with other sensitive materials in the humidity sensors, and the sensors still suffer from relatively poor performance (e.g., long response/recovery time).

Inspired by the chemical treatment of cellulose paper with trimethylammonium chloride,[29] this work directly explores the pencil-on-paper method treated with saturated NaCl solution as a high-performance humidity sensor for human health monitoring and skin characterizations. The saturated NaCl solution-treated papers as a sensing material exhibit increased ionic conductivity and significantly enhanced response. The resulting humidity sensor can conveniently monitor respiratory rate and noncontact finger locations. The continuous insensible sweat measurements also allow the sensor to characterize human skin types and evaluate skin barrier

Received: November 7, 2022
Revised: December 26, 2022
Published: December 30, 2022

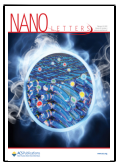

https://doi.org/10.1021/acs.nanolett.2c04384
Nano Lett. 2023, 23, 1252−1260

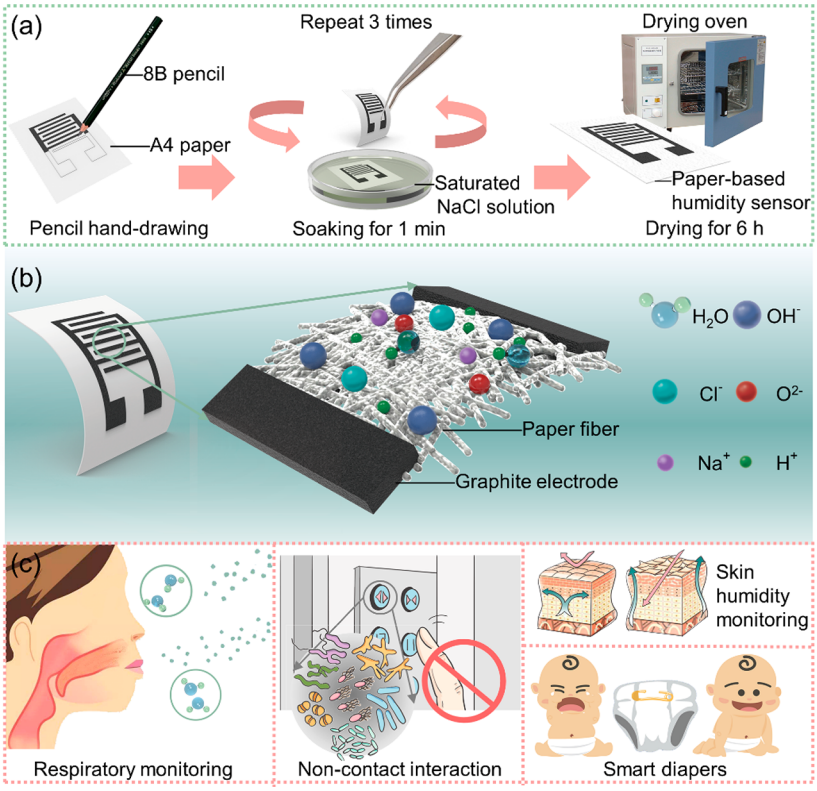

Figure 1. Fabrication and application of the pencil-on-paper hydration sensor. Schematics showing the (a) fabrication processes and (b) the response mechanism of the flexible pencil-on-paper hydration sensor with (c) applications in health monitoring, noncontact switching, and skin characterizations.

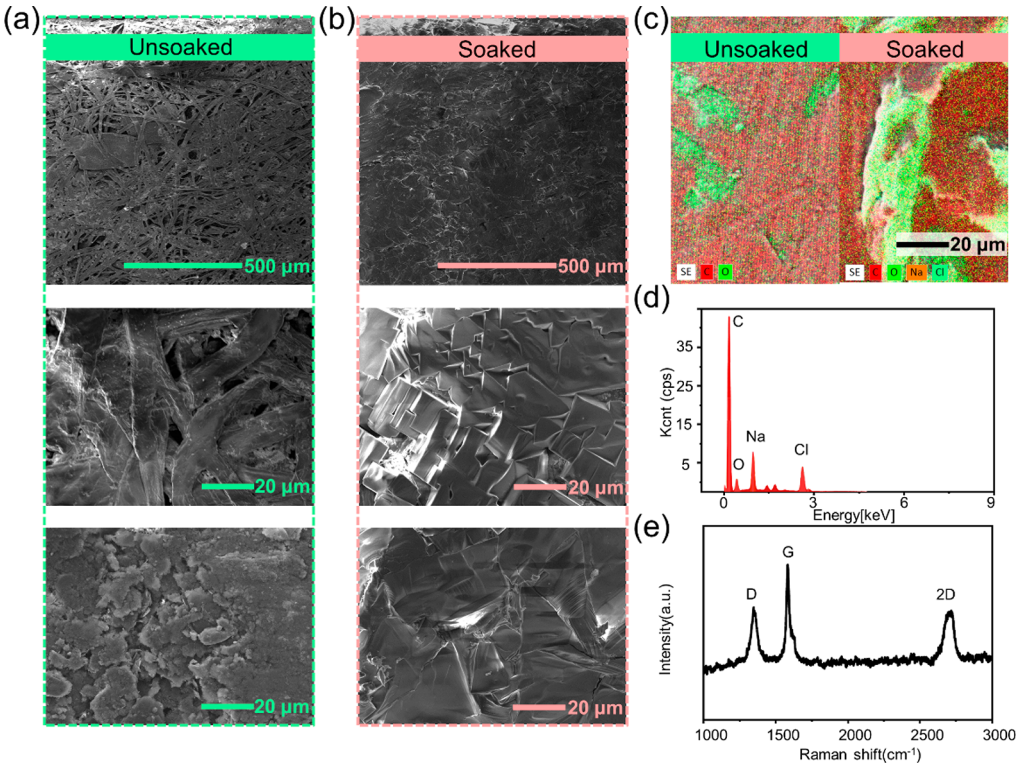

Figure 2. Structural characterization of the pencil-on-paper hydration sensor. Top view of graphite interdigital electrode on paper (a) before and (b) after treatment with NaCl solution, with magnified views shown at the bottom. (c) The energy dispersive X-ray (EDX) and (d) spectroscopy of the sensor surface after treatment. (e) Raman spectrum of the pencil trace on the paper substrate.

https://doi.org/10.1021/acs.nanolett.2c04384
Nano Lett. 2023, 23, 1252−1260

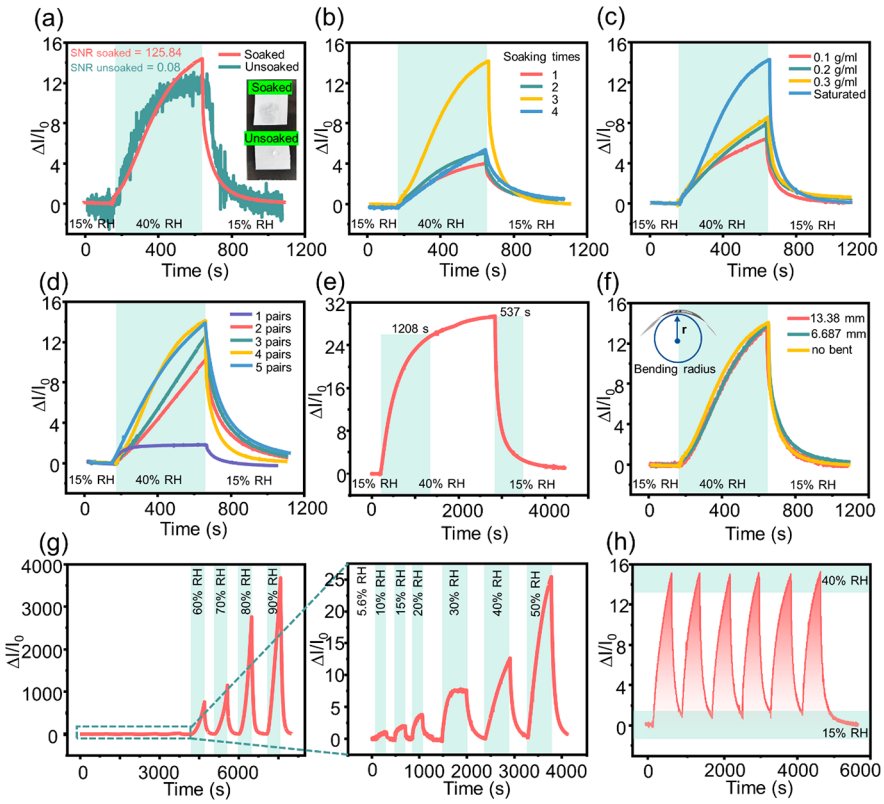

Figure 3. Optimization of the humidity sensor performance. (a) Comparison of the sensor performance before and after NaCl treatment. Effects of the (b) NaCl treatment times (at saturated concentration), (c) NaCl solution concentration (for three times of treatment), and (d) number of finger pairs in the interdigital electrodes on the sensor performance. Sensing performance characterization of the humidity sensor: (e) determination of the response and recovery time of the humidity sensor when cycled from the RH of 15% to 40% and then back to 15% and (f) effect of bending on the response (bending radius of 30° and 60°). (g) Relative current change of the humidity sensor in the RH range from 20% to 90%. Repeatability of the humidity sensor cycled between 15% RH and 40% RH (h) for six cycles (at 25 °C).

functions. The hand-drawn interdigitated electrodes with a commercial pencil on common printing papers can be easily applied in point-of-care settings, which is also suitable for mass production and is recyclable with green end products.

DESIGN AND FABRICATION OF THE PENCIL-ON-PAPER HYDRATION SENSOR

The fabrication of the sensor starts with drawing interdigitated electrodes (IDE) with a pencil on commonly used paper with a fibrous structure to facilitate the absorption and release of water molecules[30] (Figure 1a). Next, a NaCl solution immersion followed by drying allows the absorbed molecules and ions in the paper substrate to undergo ionization or hydrolysis, which facilitates the electrochemical reaction[31] across the graphite electrodes (Figure 1b and S1). The humidity sensor with high sensitivity over a large range provides application opportunities from breath monitoring and noncontact switching to smart diapers and characterizations of skin barrier functions (Figure 1c).

CHARACTERIZATION OF THE PENCIL-ON-PAPER

Before treatment, the fibrous conductive network of cellulose paper with deposited graphite (Figure 2a) can provide abundant sites for water molecule absorption. Following the treatment in saturated NaCl solution, the paper substrate is covered with dense NaCl crystals, and a layer of NaCl crystals deposited on the surface of the sensor (Figure 2b) is confirmed by the chemical composition characterized by energy dispersive X-ray (EDX) spectroscopy in Figure 2c,d. The EDX spectrum of the soaked paper clearly identifies the presence of sodium and chlorine. The cross-section morphologies of the humidity sensor indicate a uniform coating of the NaCl crystals onto cellulose fibers in the paper, and the thickness of the coated NaCl crystals increases from 35.8 to 106.2 μm as the soaking time increases from 1 to 4 times to result in increased sensor thickness from 0.17 to 0.31 mm (Figure S2). Despite different responses and signal-to-noise ratios, all of these sensors exhibit good responses at a relative humidity of 5.6% (Figure S2f). Raman spectrum of the pencil trace on paper shows three prominent peaks at 1345, 1581, and 2718 cm^{-1} (Figure 2e), which correspond to the D, G, and 2D bands of graphite.[32] The scanning electron microscope images of the electrode surface at different positions indicate uniform coating after NaCl treatment (Figure S2g–i). The small standard deviation of 7.9% in the sheet resistance from five sensors prepared from the same batch also showcases the high reproducibility of the fabrication method (Figure S3).

HUMIDITY SENSING MECHANISM

The humidity sensing exploits the hygroscopic property of cellulose paper to absorb moisture from the environment and the correlation of the moisture content of the cellulose fiber to the changes in its ionic conductivity. The type of paper substrate also affects the performance of the humidity sensor, with the response from the sensor on the Whatman No. 1 filter paper or printing paper much larger than that on the vellum or

https://doi.org/10.1021/acs.nanolett.2c04384
Nano Lett. 2023, 23, 1252−1260

Table 1. Performance Comparison of Humidity Sensors Based on Cellulose Papers

substrate	electrode material	sensitive material	response($\delta I/I$)	RH range (%)	reference
Whatman 3 mm chr	carbon ink	Whatman 3 mm chr	~10^4	20–90	22
cellulose acetate film	graphite	SiO_2	~10^4	10–93	36
printing paper	conductive adhesive tape	paper	1646	41.1–91.5	28
printing paper	graphite ink	polypyrrole	~1000	~33–90	39
cellulose filter paper	conductive adhesive tape	carbon ink	~13.50	11–98	13
printing paper	PEDOT:PVMA	PEDOT:PVMA	63.93	11–97	38
printing paper	pencil	*o*-MWCNTs	0.49	33–95	37
cellulose composite film	copper foil tape	cellulose/CNTs	2.32	11–95	35
printing paper	pencil	NaCl-modified paper	3676	5.6–90	this work

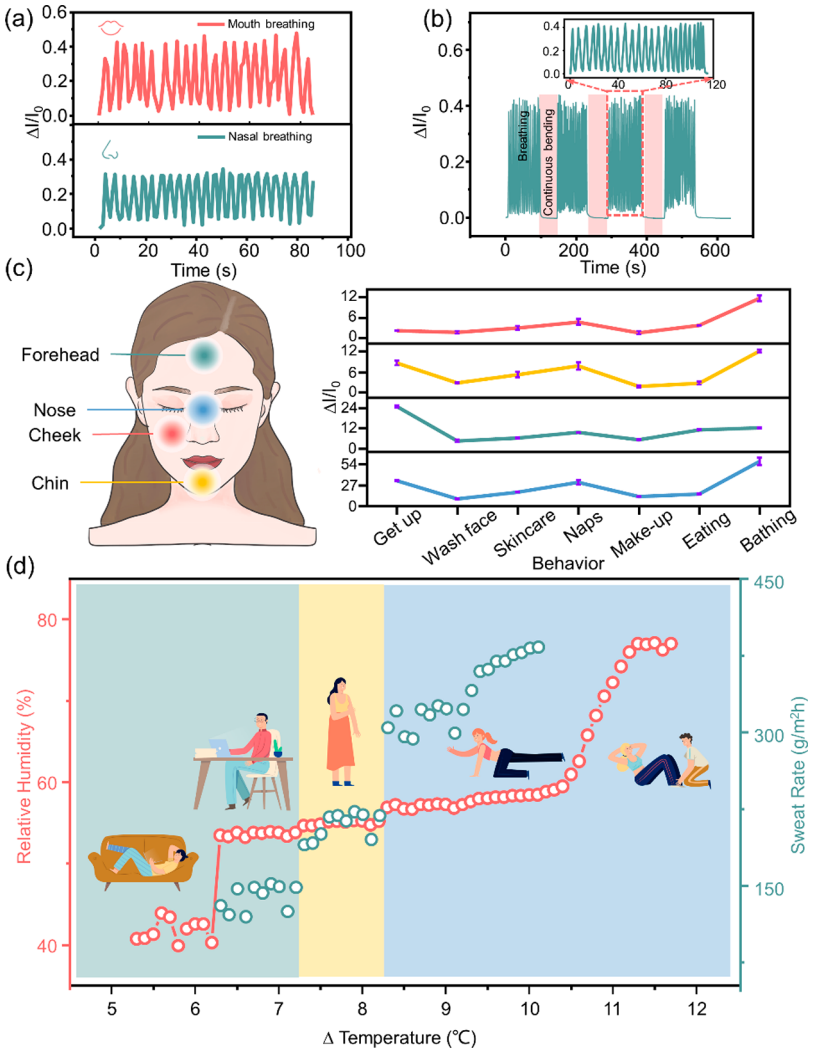

Figure 4. Application of the hydration sensor for monitoring physiological signals and characterizing the skin barrier function. (a) Comparison between mouth and nose breathing. (b) Stable response of breath monitoring before and after continuous bending. (c) Changes in the skin hydration/humidity level on the forehead, nose, cheek, and chin over varying activities during the day. (d) Measurements of sensible and insensible sweat rate as a function of the temperature difference (between the skin and ambient temperature) during lying, working, walking, doing yoga, and exercising.

sulfate paper (Figure S4). Although printing paper shows slightly lower sensitivity and slower response compared with Whatman No. 1 filter paper, it is 800 times cheaper and it is used in the following investigations unless otherwise specified. After the treatment with the NaCl solution, the sensor reduces its resistance to water vapor absorption because of the increased number of mobile electrons and enhanced ionic conductivity.[33] As a result, the sensor after NaCl treatment achieves a 1573-fold increase in the signal-to-noise ratio (SNR)[34] to a value of 125.84 (Figure 3a). Because the number of soaking times and solution concentration change the conductivity (Figure S5), they can be used to modulate the sensor response defined as the normalized relative current changes. Both the ionic conductivity and sensor response increase as the NaCl treatment is repeated up to three times because of the increased available conductive ions. However,

https://doi.org/10.1021/acs.nanolett.2c04384
Nano Lett. 2023, 23, 1252–1260

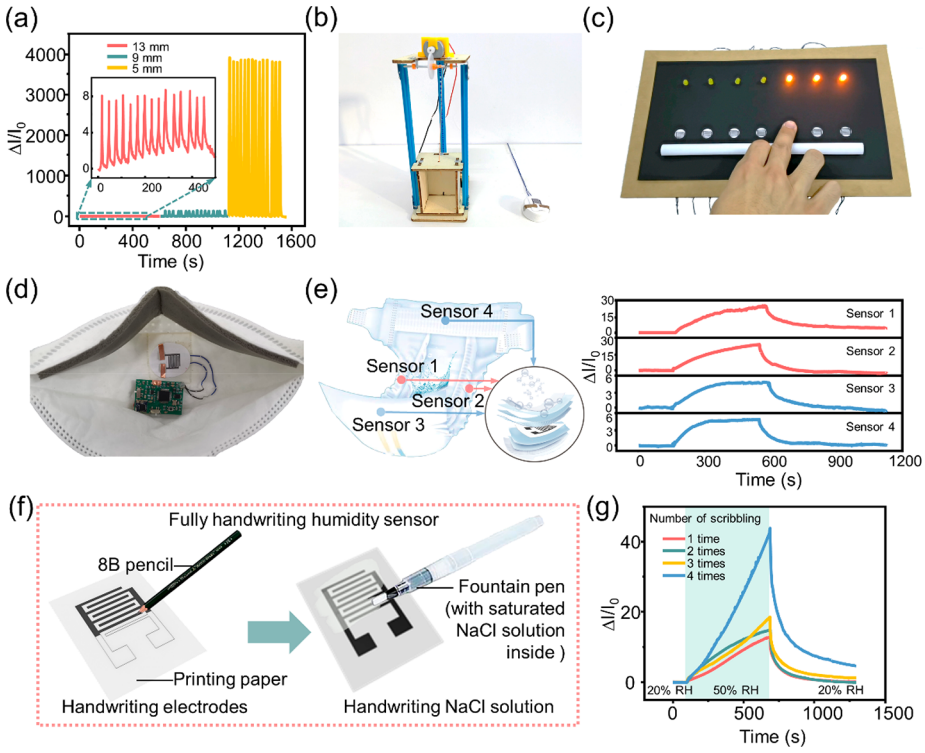

Figure 5. Application of the humidity sensor for noncontact sensing and in integrated systems. Noncontact detection of the finger for (a) proximity sensing and control of (b) the elevator and (c) LED arrays. The integrated system of (d) the smart face mask for wireless breath monitoring and telemedicine and (e) the smart diaper for monitoring the wetting process. (f) Replacement of the soaking process in the NaCl solution with a handwriting process (i.e., writing NaCl solution with a fountain pen), and (g) testing of the sensor performance at 20−50% RH.

immersion for a fourth time results in a significant reduction in both, possibly because of the formation of an overly dense NaCl layer on paper to block water contact (Figure 3b). For a given number, such as three immersion times, the increase in the NaCl solution concentration also results in increased conductivity and sensor response, with the maximum values obtained in the saturated NaCl solution (Figure 3c). Similarly, varying types of pencils are associated with different conductivities (Table S1), and the comparison indicates the 8B pencil provides the largest response (Figure S6), which is used in the following studies unless specified otherwise. Because the structural design and geometric parameters (e.g., the number of finger pairs and the gap between fingers) of the interdigital electrode also change its initial resistance, they can be used to further increase the sensitivity and response speed. The interdigital electrode with a large aspect ratio and high density of the finger pairs (four in the current design) for a given apparent area (Figure S7) exhibits the largest response (Figure 3d).

ELECTROMECHANICAL CHARACTERIZATION OF THE HUMIDITY SENSOR

When the humidity sensor is cycled between a RH of 15% and 40%, a high response of 29.23 is obtained with a response/recovery time of 1208/537 s (Figure 3e). The sensor characterization is sped up by using a short testing time of 500 s to capture the initial rapid response increase. The sensor response shows a negligibly small difference as the sensor is bent over a radius of curvature of 6 mm (Figure 3f). The flexible humidity sensor exhibits stable performance over cyclic bending, as evidenced by the negligible changes in the sensor response after 500 and 1000 bending cycles (Figure S8). The sensor can detect the RH in the range from 5.6% to 90%, with piecewise linear dependence in RH 5.6−50% (R^2 = 0.976) and RH 60−90% (R^2 = 0.965) (Figure 3g). The response in the range from RH 50% to 60% (with a slope of 0.1473 in the logarithmic fit) is much larger than the other ranges (slope of 0.0327 or 0.0244 in 5.6−50% or 60−90%) (Figure S9). The enhanced response in RH 50−60% is likely attributed to the formation of liquid water, with an increased number of free Na^+ and Cl^- from NaCl dissolved in liquid water as charge carriers for increased conductivity. The sensor also shows a highly reliable response over multiple cycles between RH 15% and 40% (Figure 3h) and a long measurement period of 30 days (Figure S10). The hydration sensor with a large response over a wide range from this work outperforms other humidity sensors on the basis of cellulose substrates (Table 1).[13,22,28,35−39]

HEALTH MONITORING AND SKIN CHARACTERIZATION

The large and fast response of the hydration sensor provides application opportunities in real-time respiration monitoring, noncontact proximity sensing, skin characterization, and smart diapers. The noncontact sensing mode of the humidity sensor used for respiratory monitoring can easily differentiate mouth breathing from nose breathing because of the difference in the current response (1.33 times greater from mouth breathing than from nose breathing, Figure 4a). The combination of the sensor response magnitude with frequency also classifies three breathing states: deep (0.12 Hz), regular (0.23 Hz), and rapid (0.57 Hz). The rapid response of the sensor allows it to detect RH cycled between 15% and 40% at frequencies of 0.04, 0.07, and 0.11 Hz (Figure S11). The sensor response in the

https://doi.org/10.1021/acs.nanolett.2c04384
Nano Lett. 2023, 23, 1252−1260

frequency domain also correlates with the noncontact dwell time of the finger on top of the sensor (Figure S12). The almost unchanged sensor response before and after bending allows its long-term use during daily activities with varying mechanical deformations (Figure 4b).

Compared with breath, the human skin exhibits a smaller change in humidity, but it can still be detected by the pencil-on-paper humidity sensor even after applying lotion or exercise (Figure S13). With a comprehensive evaluation of the skin humidity changes on the forehead, nose, chin, and cheek throughout varying activities of the day, the specific skin type of the human subject can be analyzed. The subject with a mixed, oily skin type shows higher skin humidity in the morning after waking up, followed by a decrease immediately after washing the face and slight fluctuation afterward. Comparison of the humidity variation at different places indicates a large change at the forehead and a small change at the cheek, likely because of the inherently high/low humidity on the forehead/cheek.[40] The skin humidity levels at the chin and nose also increase significantly after naps and showers (Figure 4c). The skin humidity is nonuniform across the face, with higher values in areas with less body fat (e.g., forehead, nose, and chin) and lower values in areas with more body fat, such as the cheeks.[41] The results are consistent with the mixed, oily skin type with high humidity in the T-shaped area (i.e., forehead and nose) and low humidity in the U-shaped area (i.e., cheeks and chin).[42,43] The sensor is also applicable to other human subjects (Table S2) for monitoring humidity changes during the day (Figure S14).

Sweating is the most important form of thermoregulation, which helps maintain the normal physiological activities of the body. Insensible sweating involves the evaporation of tissue fluid water from the epidermal tissue interval through the skin surface.[44] After calibration of the linear relationship between the sensor response and simulated sweat rate *in vitro* (Figure S15), as in the literature reports,[45] the hydration sensor with high sensitivity is shown to detect both sensible and insensible sweat. During low-intensity activities (e.g., lying down, working, and walking slowly), the sweat rate (SR) is observed to be lower than 150 g/m^2/h (or RH < 55%) from endogenous metabolic or stress processes. As the heat load induced by yoga or exercise increases, the body starts to secrete sensible sweat through sweat glands to the skin surface with a SR larger than 200 g/m^2/h (or RH > 55%). The transition from insensible to sensible sweat comes from the fact that the heat emitted by insensible sweat is not sufficient to regulate body temperature and sensible sweat is needed to dissipate heat.[46] The measured sweat rate (or humidity) directly reflects the change in the skin temperature (Figure 4d) because of the role of insensible/sensible sweat in the body's thermoregulation.

More importantly, the sensor can be applied in noncontact mode to detect humidity/moisture change from a distance. As the distance between the sensor and the finger decreases from 13 to 9 mm and then to 5 mm, the sensor exhibits an exponentially increased response as in ref 47 for noncontact proximity sensing (Figure 5a), which also effectively avoids the spread of bacteria from the contact. With a noncontact elevator control system consisting of a humidity sensor, a signal processing and control module (Arduino), and an elevator model (Figure 5b), the finger placed ∼5 mm above the sensor allows the wireless control of the cart (Supplementary Video 1). The array of seven humidity sensors with high sensitivity and fast response can also remotely control the ON and OFF mode of seven LEDs in the array (Figure 5c) on the basis of the circuit design provided in Figure S16. Through the use of a small humidifier, the LED array can be controlled from a large distance of 15 cm (Supplementary Video 2; for presentation purposes, the music in the video is configured by post). After combination of the sensor with a miniaturized printed circuit board (PCB) on the mask (with the schematic shown in Figure S17), the wireless respiratory monitoring system can wirelessly monitor the breathing condition/patterns in real time on a mobile phone application (Figure 5d, Supplementary Video 3). The humidity sensor can withstand various bending deformations to provide stable output signals (Figure S18). The capability to detect the onset of various disease conditions, such as respiratory arrest and shortness of breath, provides opportunities in the smart internet of things and telemedicine. The integration of four humidity sensors between the polymer absorbent layer and the water-retaining fiber layer with the data processing circuit in the diaper (Figure S19) provides a smart diaper to detect incidents of urination and wetted diapers for a timely change (Figure 5e, Supplementary Video 4). The treatment in the NaCl solution can also be achieved by filling the saturated NaCl into a fountain pen and writing gently on the electrode surface to result in a fully handwritten humidity sensor (Figure 5f). The humidity sensor prepared by this completely handwritten method exhibits the largest response (and slightly reduced SNR) after writing four times because the RH increases from 20% to 50% (Figure 5g).

In summary, this work reports a highly sensitive pencil-on-paper humidity sensor on the basis of hand-drawn graphite electrodes on cellulose paper treated with a saturated NaCl solution. The resulting humidity sensor exhibits high sensitivity, rapid response, mechanical robustness, good reproducibility, and long-term stability. Besides humidity sensing, the sensor allows sensible/insensible sweat monitoring, characterization of skin barrier functions, and noncontact sensing/control. Further combined with wireless and powering units, the integrated sensing system, as shown in the smart diapers/face masks, opens up opportunities in the design and application of next-generation devices for disease prevention and care.

Materials. The printing paper was from Deli (China), and the 8B pencil was from Mitsubishi (Japan). The sodium chloride pellets (Sinopharm Chemical Reagent Co., Ltd., China), conductive silver paste, and copper foil with a thickness of 0.05 mm were used as received.

Fabrication of the Pencil-on-Paper Humidity Sensor. The silhouette of the interdigital electrode (13.5 × 9.9 mm^2) was first drawn by AutoCAD and then printed onto the A4 printing paper. After the silhouette was filled with an 8B pencil at least 3 times, the sensor was completely immersed in the saturated NaCl solution with 8 g of NaCl pellets dissolved in 20 mL of pure water. The electrode was soaked while facing down for ca. 40 s and while facing up for another 20 s and then dried in a drying machine at 80 °C for 20 min. After this procedure was repeated for a given number of cycles, the fabrication was completed by connecting both ends of interdigital electrodes to a digital source meter (connected to a computer) with copper wires and conductive silver paste. Fabrication of the fully handwritten electrode was achieved by filling a saturated NaCl solution into a fountain pen, writing

https://doi.org/10.1021/acs.nanolett.2c04384
Nano Lett. 2023, 23, 1252−1260

gently on the electrode surface (8B pencil electrodes), and then drying at 80 °C for 20 min.

Humidity Testing System. The testing of the humidity sensors used the saturated salt solution method, which included a saturated salt solution and a commercial hygrometer in a testing chamber. The humidity sensor was first placed inside the testing chamber with a specific relative humidity generated by different saturated salt solutions (5.6%, 10%, 15%, 20%, and 30% RH by using LiBr; 40%, 50%, 60%, and 65% RH by using NaCl; and 70%, 80%, and 90% RH by using KCl) in their equilibrium states. The current readout of the sensor was recorded with the I−V Software in real time (frequency of 1 Hz and voltage of 1 V).

Characterization of the Humidity Sensor for Insensible/Sensible Sweat Sensing. The evaporation of water through the Whatman No. 1 filter paper provides the setup for the simulated sweat, with the rate controlled by the water volume at a given temperature (Figure S20). The relative humidity was measured every 5 min and the weight change was measured by a precision electronic scale every 10 min.[48] The water evaporation or simulated sweat rate (SR) was then calculated from at least three measurements according to $\mathrm{SR}\,[\mathrm{g}/(\mathrm{m}^2/\mathrm{h})] = \frac{W\,[g]}{A\,[m^2]\times T\,[h]}$,[49] where W is the weight of water loss, A is the area of the tube, and T is the time. With a water volume in the range of 10 to 50 mL at a temperature ranging from 25 to 95 °C, the sweat rate can be controlled to be in a wide range from 7.09 to 660.42 g/(m^{2}h). The measured sweat rate was observed to depend linearly on the relative humidity.[47]

Human Subject Testing. For the mouth breathing test, a tissue was used to cover both nostrils, and the sensor was placed about 8 mm in front of the slightly opened mouth. For the nose breathing test, the mouth was closed, and the sensor was placed about 8 mm below the nose. In the test to measure the mechanical robustness, the sensor was bent 50 s after the measurement of continuous breathing for about 100 s, and then the breath testing was continued. The experiment to characterize the facial skin conditions (or barrier functions) over a day was carried out at an ambient temperature of 25 °C and relative humidity of 45 ± 5%. The subjects were asked to keep their skincare habits. The face of each subject was washed with a commercially available cleansing product, then each subject was placed in the environmental chamber at constant temperature and humidity for 10 min to normalize the skin condition. The skincare and measurement were carried out 10 min (or 20 min) after the application of commercially available moisturizing products (or after bathing) with the humidity sensor in a semienclosed chamber. The ambient temperature and relative humidity level were kept constant at 25 ± 1 °C and 45 ± 5%, respectively. Napping was performed for about 30 min, and the same food was consumed for all subjects. The four sensors were placed around the diaper during the simulated urination experiment, and the test device was placed on the inside of the human arm during the experiment with insensible sweat (Figure S21).

Wireless Respiratory Monitoring System. Integration of the humidity sensor on the face mask with the Microcontroller Unit (MCU, STM32F103C8T6, STMicroelectronics), Bluetooth Low Energy (BLE, RF-BM-4044B4, Xinchida), and a power supply (300 mAh micropolymer lithium battery) yielded the wireless respiratory monitoring system. For the operating voltage of 3.3 V, the operating current of the MCU and BLE was 20 and 6 mA, respectively. With negligible energy consumption in other components, the operation time of the wireless system powered by the 300 mAh micropolymer lithium battery can be estimated to be 11.54 h. The BLE module in the wireless system has a maximum communication distance of 150 m, a transmission rate of 16 k/s, and a minimum transmission interval of 10 ms.

The four sensors were placed around the diaper during the simulated urination experiment, and the test device was placed on the inside of the human arm during the experiment with insensible sweat.

■ ASSOCIATED CONTENT

Supporting Information

The Supporting Information is available free of charge at https://pubs.acs.org/doi/10.1021/acs.nanolett.2c04384.

Photographs of the sensor and integrated devices; characterization of sensors prepared by different methods; sheet resistance of five sensors from the same batch; response of the moisture sensor on different paper substrates; characterization of the sensor prepared with different pencils; dependence of sensor response on the relative humidity; application of the hydration sensor and integrated devices for physiological signal monitoring, noncontact sensing characterization of the skin barrier function, and insensible/sensible sweat rate; circuit diagram of the integrated systems; demonstrations of the robust performance of the wireless respiratory monitoring system upon mechanical deformations; experimental setup for measuring the simulated sweating rate; and tables of the electrical properties of the pencil trace on the printing paper and the human subject information (PDF)

Operation of noncontact elevator control system (MP4)

Control of LED array from 15 cm (MP4)

Wireless respiratory monitoring system on a mobile phone application (MP4)

Smart diaper detection of incidents of urination and wetted diapers (MP4)

■ AUTHOR INFORMATION

Corresponding Authors

Huanyu Cheng − *Department of Engineering Science and Mechanics, The Pennsylvania State University, University Park, Pennsylvania 16802, United States;* orcid.org/0000-0001-6075-4208; Email: huanyu.cheng@psu.edu

Li Yang − *State Key Laboratory of Reliability and Intelligence of Electrical Equipment, School of Health Sciences and Biomedical Engineering, Hebei University of Technology, Tianjin 300130, China; Tianjin Tianzhong Yimai Technology Development Co. Ltd., Tianjin 300384, China;* orcid.org/0000-0001-6798-3177; Email: yangli5781@126.com

Authors

Guangyu Niu − *Department of Architecture and Art, Hebei University of Technology, Tianjin 300130, China*

Zihan Wang − *State Key Laboratory for Reliability and Intelligence of Electrical Equipment, Hebei Key Laboratory of Smart Sensing and Human-Robot Interaction, School of Mechanical Engineering, Hebei University of Technology, Tianjin 300401, China*

Ye Xue − *State Key Laboratory of Reliability and Intelligence of Electrical Equipment, School of Health Sciences and Biomedical Engineering, Hebei University of Technology, Tianjin 300130, China*
Jiayi Yan − *State Key Laboratory for Reliability and Intelligence of Electrical Equipment, Hebei Key Laboratory of Smart Sensing and Human-Robot Interaction, School of Mechanical Engineering, Hebei University of Technology, Tianjin 300401, China*
Ankan Dutta − *Department of Engineering Science and Mechanics, The Pennsylvania State University, University Park, Pennsylvania 16802, United States*
Xue Chen − *State Key Laboratory of Reliability and Intelligence of Electrical Equipment, Key Laboratory of Bioelectromagnetics and Neuroengineering of Hebei Province, School of Electrical Engineering, Hebei University of Technology, Tianjin 300130, China*
Ya Wang − *State Key Laboratory for Reliability and Intelligence of Electrical Equipment, Hebei Key Laboratory of Smart Sensing and Human-Robot Interaction, School of Mechanical Engineering, Hebei University of Technology, Tianjin 300401, China*
Chaosai Liu − *State Key Laboratory for Reliability and Intelligence of Electrical Equipment, Hebei Key Laboratory of Smart Sensing and Human-Robot Interaction, School of Mechanical Engineering, Hebei University of Technology, Tianjin 300401, China*
Shuaijie Du − *State Key Laboratory of Reliability and Intelligence of Electrical Equipment, Key Laboratory of Bioelectromagnetics and Neuroengineering of Hebei Province, School of Electrical Engineering, Hebei University of Technology, Tianjin 300130, China*
Langang Guo − *State Key Laboratory for Reliability and Intelligence of Electrical Equipment, Hebei Key Laboratory of Smart Sensing and Human-Robot Interaction, School of Mechanical Engineering, Hebei University of Technology, Tianjin 300401, China*
Peng Zhou − *Tianjin Tianzhong Yimai Technology Development Co. Ltd., Tianjin 300384, China*

Complete contact information is available at: https://pubs.acs.org/10.1021/acs.nanolett.2c04384

Author Contributions

[¶]These authors contributed equally to this work.

Notes

The authors declare no competing financial interest.

■ ACKNOWLEDGMENTS

This work was supported by the National Natural Science Foundation of China (51705126, 61871173), the Key Research and Development Project of Hebei Province (20271701D, 22371703D), China Postdoctoral Science Foundation (2022M722378), and the Innovation Financing Program for Postgraduates of Hebei Province (CXZZSS2022052). H.C. acknowledges the support provided by NIH (Award Nos. R21EB030140, U01DA056242, and R61HL154215), NSF (Grant No. ECCS-1933072), and Penn State University.

■ REFERENCES

(1) Yang, L.; Yi, N.; Zhu, J.; Cheng, Z.; Yin, X.; Zhang, X.; Zhu, H.; Cheng, H. Novel gas sensing platform based on a stretchable laser-induced graphene pattern with self-heating capabilities. *J. Mater. Chem. A* **2020**, *8* (14), 6487−6500.
(2) Wakabayashi, S.; Arie, T.; Akita, S.; Nakajima, K.; Takei, K. A multitasking flexible sensor via reservoir computing. *Adv. Mater.* **2022**, *34* (26), 2201663.
(3) Zhang, T.; Wang, Z.; Srinivasan, B.; Wang, Z.; Zhang, J.; Li, K.; Boussard-Pledel, C.; Troles, J.; Bureau, B.; Wei, L. Ultraflexible glassy semiconductor fibers for thermal sensing and positioning. *ACS Appl. Mater. Interfaces* **2019**, *11* (2), 2441−2447.
(4) Lan, L.; Le, X.; Dong, H.; Xie, J.; Ying, Y.; Ping, J. One-step and large-scale fabrication of flexible and wearable humidity sensor based on laser-induced graphene for real-time tracking of plant transpiration at bio-interface. *Biosens. Bioelectron.* **2020**, *165*, 112360.
(5) Tai, H.; Duan, Z.; Wang, Y.; Wang, S.; Jiang, Y. Paper-based sensors for gas, humidity, and strain detections: A Review. *ACS Appl. Mater. Interfaces* **2020**, *12* (28), 31037−31053.
(6) Marc, M.; Ignacio, G.; Raul, F. A smart textile system to detect urine leakage. *IEEE Sens. J.* **2021**, *21* (23), 26234−26242.
(7) Zhao, H.; Wang, Z.; Li, Y.; Yang, M. Single-sided and integrated polyaniline poly(vinylidene fluoride) flexible membrane with micro nanostructures as breathable, nontoxic and fast response wearable humidity sensor. *J. Colloid Interface Sci.* **2022**, *607* (1), 367−377.
(8) Dong, H.; Li, D.; Pang, J.; Zhang, Q.; Xie, J. Highly sensitive and fast-response humidity sensor based on saw resonator and mos_2 for human activity detection. *2021 IEEE 34th International Conference on Micro Electro Mechanical Systems (MEMS)* **2021**, 322−325.
(9) Li, T.; Li, L.; Sun, H.; Xu, Y.; Wang, X.; Luo, H.; Liu, Z.; Zhang, T. Porous ionic membrane based flexible humidity sensor and its multifunctional applications. *Adv. Sci.* **2017**, *4* (5), 1600404.
(10) Yang, L.; Ji, H.; Meng, C.; Li, Y.; Zheng, G.; Chen, X.; Niu, G.; Yan, J.; Xue, Y.; Guo, S.; Cheng, H. Intrinsically breathable and flexible NO_2 gas sensors produced by laser direct writing of self-assembled block copolymers. *ACS Appl. Mater. Interfaces* **2022**, *14* (15), 17818−17825.
(11) Chen, X.; Li, R.; Niu, G.; Xin, M.; Xu, G.; Cheng, H.; Yang, L. Porous graphene foam composite-based dual-mode sensors for underwater temperature and subtle motion detection. *Chem. Eng. J.* **2022**, *444*, 136631.
(12) Zhao, J.; Yu, Z.; Tu, Z.; Bian, H. Influence of electrode structure on performance of laser direct writing Cu-PI flexible humidity sensor. *Micromachines* **2022**, *13* (7), 992.
(13) Li, X.; Guo, Y.; Meng, J.; Li, X.; Li, M.; Gao, D. Self-powered carbon ink/filter paper flexible humidity sensor based on moisture-induced voltage generation. *Langmuir* **2022**, *38* (27), 8232−8240.
(14) Zhang, T.; Zhang, S.; Gu, Z.; Zhao, R.; Wang, S.; Guo, L.; Li, T.; Zhang, Y.; Song, Y. Pen-writing high-quality perovskite films and degradable optoelectronic devices. *RSC. Adv.* **2022**, *12*, 3924−3930.
(15) Ma, L.; Wu, R.; Patil, A.; Zhu, S.; Meng, Z.; Meng, H.; Hou, C.; Zhang, Y.; Liu, Q.; Yu, R.; Wang, J.; Lin, N.; Liu, X. Y. Full-textile wireless flexible humidity sensor for human physiological monitoring. *Adv. Funct. Mater.* **2019**, *29* (43), 1904549.
(16) He, Y.; Zhang, M.; Zhang, N.; Zhu, D.; Huang, C.; Kang, L.; Zhou, X.; Hu, M.; Zhang, J. Paper-based ZnS: Cu alternating current electroluminescent devices for current humidity sensors with high-linearity and flexibility. *Sensors* **2019**, *19* (21), 4607.
(17) Li, Z.; Wang, J.; Xu, Y.; Shen, M.; Duan, C.; Dai, L.; Ni, Y. Green and sustainable cellulose-derived humidity sensors: A review. *Carbohydr. Polym.* **2021**, *270*, 118385.
(18) Liu, H.; Xiang, H.; Wang, Y.; Li, Z.; Qian, L.; Li, P.; Ma, Y.; Zhou, H.; Huang, W. A flexible multimodal sensor that detects strain, humidity, temperature, and pressure with carbon black and reduced graphene oxide hierarchical composite on paper. *ACS Appl. Mater. Interfaces* **2019**, *11* (43), 40613−40619.
(19) Yang, L.; Wang, H.; Yuan, W.; Li, Y.; Gao, P.; Tiwari, N.; Chen, X.; Wang, Z.; Niu, G.; Cheng, H. Wearable pressure sensors based on MXene/tissue papers for wireless human health monitoring. *ACS Appl. Mater. Interfaces* **2021**, *13* (50), 60531−60543.

(20) Chen, X.; Li, Y.; Wang, X.; Yu, H. Origami paper-based stretchable humidity sensor for textile-attachable wearable electronics. *ACS Appl. Mater. Interfaces* **2022**, *14* (31), 36227−36237.
(21) Prebianto, N.; Futra, A.; Ieee. Paper as a substrate for sensor applications: a review. *2018 International Conference on Applied Engineering (ICAE)* **2018**, 1−5.
(22) Guder, F.; Ainla, A.; Redston, J.; Mosadegh, B.; Glavan, A.; Martin, T.; Whitesides, G. Paper-based electrical respiration sensor. *Angew. Chem., Int. Ed.* **2016**, *55* (19), 5727−5732.
(23) Duan, Z.; Jiang, Y.; Huang, Q.; Wang, S.; Wang, Y.; Pan, H.; Zhao, Q.; Xie, G.; Du, X.; Tai, H. Paper and carbon ink enabled low-cost, eco-friendly, flexible, multifunctional pressure and humidity sensors. *Smart Materials* **2021**, *30* (5), 055012.
(24) Wang, S.; GU, Z.; Zhao, R.; Zhang, T.; Lou, Y.; Guo, L.; Su, M.; Li, L.; Zhang, Y.; Song, Y. A general method for growth of perovskite single-crystal arrays for high performance photodetectors. *Nano Research* **2022**, *15* (7), 6568−6573.
(25) Turkani, V.; Maddipatla, D.; Narakathu, B.; Saeed, T.; Obare, S.; Bazuin, B.; Atashbar, M. A highly sensitive printed humidity sensor based on a functionalized MWCNT/HEC composite for flexible electronics application. *Nanoscale Advances* **2019**, *1* (6), 2311−2322.
(26) Muslu, E.; Eren, E.; Oksuz, A. U. Prussian blue-based flexible thin film nanoarchitectonics for non-enzymatic electrochemical glucose sensor. *J. Inorg. Organomet Polym. Mater.* **2022**, *32* (8), 2843−2852.
(27) Kanaparthi, S. Pencil-drawn paper-based non-invasive and wearable capacitive respiration sensor. *Electroanalysis* **2017**, *29* (12), 2680−2684.
(28) Duan, Z.; Jiang, Y.; Yan, M.; Wang, S.; Yuan, Z.; Zhao, Q.; Sun, P.; Xie, G.; Du, X.; Tai, H. Facile, flexible, cost-saving, and environment-friendly paper-based humidity sensor for multifunctional applications. *ACS Appl. Mater. Interfaces* **2019**, *11* (24), 21840−21849.
(29) Guan, X.; Hou, Z.; Wu, K.; Zhao, H.; Liu, S.; Fei, T.; Zhang, T. Flexible humidity sensor based on modified cellulose paper. *Sens. Actuators B Chem.* **2021**, *339*, 129879.
(30) Mohammadzadeh, A.; Barletta, M.; Gisario, A. Manufacturing of cellulose-based paper: dynamic water absorption before and after fiber modifications with hydrophobic agents. *Appl. Phys. A: Mater. Sci. Process.* **2020**, *126* (5), 383.
(31) Zhang, Y.; Duan, Z.; Zou, H.; Ma, M. Drawn a facile sensor: A fast response humidity sensor based on pencil-trace. *Sens. Actuators B Chem.* **2018**, *261*, 345−353.
(32) Liao, X.; Liao, Q.; Yan, X.; Liang, Q.; Si, H.; Li, M.; Wu, H.; Cao, S.; Zhang, Y. Flexible and highly sensitive strain sensors fabricated by pencil drawn for wearable monitor. *Adv. Funct. Mater.* **2015**, *25* (16), 2395−2401.
(33) Steffens, C.; Manzoli, A.; Paschoalin, R.; Tiggemann, L.; Steffens, J.; Teixeira, E.; Herrmann, P. Tracing paper substrate used for development of interdigitated graphite electrode and its application as humidity sensor. *Synth. Met.* **2013**, *183*, 36−39.
(34) Yang, L.; Zheng, G.; Cao, Y.; Meng, C.; Li, Y.; Ji, H.; Chen, X.; Niu, G.; Yan, J.; Xue, Y.; Cheng, H. Moisture-resistant, stretchable NO_x gas sensors based on laser-induced graphene for environmental monitoring and breath analysis. *Microsyst. Nanoeng.* **2022**, *8*, 78.
(35) Zhu, P.; Liu, Y.; Fang, Z.; Kuang, Y.; Zhang, Y.; Peng, C.; Chen, G. Flexible and highly sensitive humidity sensor based on cellulose nanofibers and carbon nanotube composite film. *Langmuir* **2019**, *35* (14), 4834−4842.
(36) Kano, S.; Fujii, M. All-Painting Process to produce respiration sensor using humidity-sensitive nanoparticle film and graphite trace. *ACS Sustain. Chem. Eng.* **2018**, *6* (9), 12217−12223.
(37) Zhao, H.; Zhang, T.; Qi, R.; Dai, J.; Liu, S.; Fei, T. Drawn on Paper: A reproducible humidity sensitive device by handwriting. *ACS Appl. Mater. Interfaces* **2017**, *9* (33), 28002−28009.
(38) Yuan, Y.; Zhang, Y.; Liu, R.; Liu, J.; Li, Z.; Liu, X. Humidity sensor fabricated by inkjet-printing photosensitive conductive inks PEDOT: PVMA on a paper substrate. *RSC Adv.* **2016**, *6* (53), 47498−47508.
(39) Santhiago, M.; da Costa, P. G.; Pereira, M. P.; Correa, C. C.; de Morais, V. B.; Bufon, C. C.B. Versatile and robust integrated sensors to locally assess humidity changes in fully enclosed paper-based devices. *ACS Appl. Mater. Interfaces* **2018**, *10* (41), 35631−35638.
(40) Egawa, M.; Koizumi, K.; Hirao, T. Changes in facial moisture distribution and feelings of moisture/dryness among various environmental temperatures and humidities in summer and winter. *Skin Res. Technol.* **2020**, *26* (6), 937−948.
(41) Anderson, K.; Oleson, J.; Anthony, T. Variability in coefficient of restitution in human facial skin. *Skin Res. Technol.* **2014**, *20* (3), 355−362.
(42) Wan, M.; Su, X.; Zheng, Y.; Gong, Z.; Yi, J.; Zhao, Y.; Guan, X.; Lai, W. Seasonal variability in the biophysical properties of forehead skin in women in Guangzhou City, China. *Int. J. Dermatol.* **2015**, *54* (11), 1319−1324.
(43) Yi, F.; Yang, X.; Yang, R.; Zhao, M.; Dong, Y.; Li, L.; He, Y.; Guo, M.; Li, J.; Zhang, X.; Lu, Z.; Gu, J.; Bao, J.; Meng, H. A cross-sectional study of Chinese women facial skin status with environmental factors and individual lifestyles. *Sci. Rep.* **2022**, *12* (1), 18110−18110.
(44) Zhong, B.; Jiang, K.; Wang, L.; Shen, G. Wearable sweat loss measuring devices: from the role of sweat loss to advanced mechanisms and designs. *Adv. Sci.* **2022**, *9* (1), e2103257.
(45) Nilsson, G. Measurement of water exchange through skin. *Med. Bio Eng. Comput* **1977**, *15* (3), 209−218.
(46) Lin, S.; Wang, B.; Zhao, Y.; Shih, R.; Cheng, X.; Yu, W.; Hojaiji, H.; Lin, H.; Hoffman, C.; Ly, D.; Tan, J.; Chen, Y.; Di Carlo, D.; Milla, C.; Emaminejad, S. Natural perspiration sampling and in situ electrochemical analysis with hydrogel micropatches for user-identifiable and wireless chemo/biosensing. *ACS Sens.* **2020**, *5* (1), 93−102.
(47) Schwindt, D.; Wilhelm, K.; Maibach, H. Water diffusion characteristics of human stratum corneum at different anatomical sites in vivo. *J. Infect. Dis.* **1998**, *111* (3), 385−389.
(48) Sim, J.; Cho, Y. Portable sweat rate sensors integrated with air ventilation actuators. *Sens. Actuators B Chem.* **2016**, *234*, 176−183.
(49) Sim, J.; Yoon, S.; Cho, Y. Wearable sweat rate sensors for human thermal comfort monitoring. *Sci. Rep.* **2018**, *8* (1), 1181.

https://doi.org/10.1021/acs.nanolett.2c04384
Nano Lett. 2023, 23, 1252−1260